In Vitro and In Vivo Evaluation of a Technetium-99m-Labeled 2-Nitroimidazole (BMS181321) as a Marker of Tumor Hypoxia

James R. Ballinger, Judy Wan Min Kee and Andrew M. Rauth
Divisions of Nuclear Medicine and Experimental Therapeutics, Ontario Cancer Institute/Princess Margaret Hospital; Departments of Pharmacy, Medicine and Medical Biophysics, University of Toronto, Toronto, Canada

The ^{99m}Tc-labeled 2-nitroimidazole derivative BMS181321, previously studied in experimental models of myocardial and cerebral ischemia, has been evaluated in single-cell and tumor models. **Methods:** Accumulation of BMS181321 was studied in aerobic and hypoxic (<10 PPM O_2) suspension cultures of Chinese hamster ovary (CHO) cells at 37°C and the oxygen dependency and stability of the accumulated radioactivity determined. Biodistribution studies of the tracer after intravenous injection in C3H mice bearing three different murine solid tumors were performed noninvasively using a gamma camera, as well as invasively by determining blood and tissue levels of radioactivity from 10 min to 24 hr after injection. **Results:** Accumulation of BMS181321 in aerobic cells in vitro equilibrated within 5 min at a ~10-fold level over the external medium. Hypoxic cells showed a linear increase in radioactivity up to 4 hr for cell densities $\leq 1 \times 10^6$/ml. At higher cell densities ($2–4 \times 10^6$/ml) there was substantial depletion of radioactivity from the growth medium and increased alteration in the chemical state of the tracer that remained. Low O_2 levels (~40 ppm) inhibited the maximal accumulation rate by 50%. Approximately 30% of radioactivity accumulated under hypoxic conditions remained cell-associated after 24 hr. Following intravenous injection, the tracer rapidly distributed throughout the mouse and was predominately cleared through the hepatobiliary system. Blood levels of radioactivity cleared quickly and plateaued at ~4% of the total dose from 2–24 hr. Absolute uptake in the tumors was highest 10 min after injection, and the tumor-to-muscle activity ratios increased and plateaued from 4–8 hr at values of 3.5–4.0. Two drugs which affect blood flow and increase hypoxic cell fraction in these tumors, hydralazine and nitro-L-arginine, significantly increased levels of BMS181321 radioactivity over control levels with minimal effects on normal tissue retention. **Conclusion:** These results suggest BMS181321 or an analog of it will be a useful agent to investigate the status of hypoxia in solid tumors experimentally and potentially in the clinic.

Key Words: nitroimidazole; technetium-99m; hypoxia; tumors

J Nucl Med 1996; 37:1023–1031

Hypoxia in tumors may be an important factor in resistance to radiotherapy and chemotherapy (*1,2*). Detection of tumor hypoxia by radionuclide imaging techniques was proposed by Chapman in 1979 (*3*) using radiolabeled 2-nitroimidazoles which are reduced enzymatically and trapped in regions of low oxygen tension. Since then, ^{18}F-fluoromisonidazole (FMISO) has been developed and evaluated for detecting hypoxia in tumors (*4*) and myocardium (*5*) with PET. Wiebe et al. investigated a series of ^{123}I-labeled 2-nitroimidazole derivatives for imaging with the more widely available SPECT, culminating with ^{123}I-iodoazomycin arabinoside (IAZA) which is in clinical trials (*6–8*). Krohn prepared iodovinylmisonidazole and evaluated it in animals (*9,10*).

Received May 24, 1995; accepted Jul. 28, 1995.
For correspondence or reprints contact: James R. Ballinger, PhD, Department of Nuclear Medicine, Ontario Cancer Institute, 610 University Ave., Toronto, Ontario, Canada, M4G5 2M9.

Since ^{99m}Tc is the workhorse of nuclear medicine, there has been considerable interest in developing a ^{99m}Tc-labeled 2-nitroimidazole derivative. Such an agent, BMS181321 (Oxo[[3,3,9,9-tetramethyl-1-(2-nitro-1H-imidazol-1-yl)-4,8-diazaundecane-2,10-dione dioximato](3-)-N,N′,N″,N‴]-technetium), in which 2-nitroimidazole is linked to a propylene amine oxime (PnAO) chelator (Fig. 1), was reported in 1992 (*11–13*) and has been evaluated in experimental models of myocardial and cerebral ischemia (*14–16*). The use of this agent to detect hypoxia in tumors, however, has not yet been reported.

In the present work the applicability of BMS181321 for imaging tumor hypoxia has been evaluated. The properties of BMS181321 have been studied in an in vitro system to determine the kinetics of accumulation in aerobic versus hypoxic cells in suspension culture, the O_2 dependency of this accumulation and the stability of the accumulated activity in cells. The biodistribution of BMS181321, after intravenous injection in C3H mice bearing three different transplanted murine tumors, was studied to assess the accumulation of the tracer in tumors as a function of time after injection, size of tumor and type of tumor. In addition, the effects of two putative pharmacological modulators of tumor hypoxia, hydralazine (*17*) and nitro-L-arginine (*18*), were tested. The results of these studies support several potential applications of BMS181321, both experimentally and clinically.

MATERIALS AND METHODS

Preparation of BMS181321

The ^{99m}Tc-labeled 2-nitroimidazole BMS181321 was prepared from kits supplied by Bristol-Myers Squibb (*13*). Two milligrams of the lyophilized ligand, BMS181032, were dissolved in 2 ml saline containing 740 MBq (20 mCi) ^{99m}Tc-pertechnetate. A stannous DTPA kit was reconstituted with 4 ml saline, an aliquot of 0.15 ml was removed and added to the vial containing the ligand and pertechnetate. After 10 min at room temperature the radiochemical purity of BMS181321 was determined by paper chromatography using a strip from a solvent saturation pad. The strip was prespotted with ethanol followed immediately by BMS181321, and then developed in diethyl ether. The lipophilic BMS181321 complex migrates to the top half of the strip while the hydrophilic and/or insoluble radiochemical impurities remain near the origin (*19*). Radiochemical purity was >90%. The radiopharmaceutical was further diluted with saline to a concentration of 10 MBq/ml and used within 30 min of preparation. The optical density of the BMS181321 solution was monitored at 323 nm, the absorption peak of the 2-nitroimidazole, as a function of time after preparation.

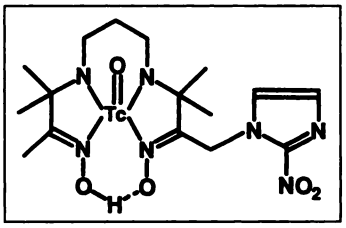

FIGURE 1. Structure of BMS181321, ^{99m}TcO(PnAO)-1-2-nitroimidazole.

Cells

Cells used in these experiments were Chinese hamster ovary (CHO) cells subclone AA8-4 grown in suspension culture at 37°C in α-medium plus 10% fetal calf serum. Cells were used in the exponential phase of growth and doubling times were 11–14 hr. Cell viability was assessed by a colony-formation assay by plating cells in growth medium and incubating for eight days at 37°C, staining with methylene blue and counting colonies of 50 or more cells. Plating efficiency was 70–90%.

Accumulation of BMS181321 in Cells

CHO cells were spun down from suspension culture and resuspended in fresh growth medium at the desired cell density (0.1–5 × 10^6/ml). Cells (9.7 ml) were equilibrated for 30 min in glass vials as stirred cell suspensions with a continual flow of a prehumidified gas mixture of N_2 containing 5% CO_2 and <10 ppm O_2 (hypoxic exposure) or 5% CO_2 and 95% air (aerobic exposure) as previously described (*20*). After equilibration, 0.3 ml of BMS181321 was added to yield a final radioactivity and mass concentration of tracer and ligand of ~0.25 MBq/ml and 0.7 μg/ml, respectively. At various times after addition of the tracer, 0.3–0.5 ml samples were removed from the vials without disturbing the oxygenation status of cells in the vial. This was done to determine the tracer accumulation in the cells. Typically, 0.1-ml aliquots of the vial sample were layered in duplicate over an oil gradient and centrifuged (*21*). The aqueous growth medium layer and ~90% of the oil layer were then carefully aspirated and the tube tip containing the cell pellet and remaining oil was clipped into a counting tube and assayed in a gamma well counter.

A series of control experiments with cells which had accumulated BMS181321 demonstrated that cell recovery was efficient (>99%) and linear from 1 × 10^4 to 5 × 10^5 cells using the spin-through-oil technique. A small carry-through of radioactivity from the growth medium to which BMS181321 was added was noted which was approximately 0.7% of the counts in 0.1 ml of radioactive medium. A correction was made in cell accumulation studies for this carry-through where appropriate.

In order to assess the status of the radioactivity left in the supernatant on the top of the oil layer after the cells were spun through, aliquots of supernatants were placed in tubes containing 2 ml ethyl acetate and 2 ml PBS at room temperature. The tubes were capped, vortexed for 30 sec and then centrifuged briefly (200 g, 30 sec) to separate the phases. The phases were pipetted into separate tubes and assayed in the gamma well counter. The percent extracted into the organic phase was calculated as the counts in the ethyl acetate divided by total counts in both phases (i.e., total supernatant counts). In control experiments in which BMS181321 was added to growth medium without cells and incubated at 37°C under aerobic or hypoxic conditions, there was <5% decrease in the percentage extracted (~90%) over the course of 5 hr.

The ratio of the radioactivity in 0.1 ml of packed cells (CPM_{in} or C_{in}) to the radioactivity in 0.1 ml of growth medium (CPM_{out} or C_{out}) could be calculated and the data are presented in the form of this ratio, abbreviated to C_{in}/C_{out}. Previous experiments have shown no change in CHO cell volume as a result of hypoxic or aerobic incubation alone up to 5 hr (*21*).

Oxygen Dependency of BMS181321 Accumulation

The role of O_2 in modulating uptake and accumulation of BMS181321 was assessed as described previously for the accumulation of the 2-nitroimidazole misonidazole (*20*). Briefly, a 40-ml polyshell glass vial was fitted with a silicone stopper through which an O_2 sensor designed, constructed and kindly supplied by C.J. Koch, PhD, (University of Pennsylvania, Philadelphia, PA) and/or gas inlet and outlet were inserted. A small magnetic bar stirred the 10-ml cell suspension in the vial. The gas inlet was connected through a humidifying chamber and flow regulators which could be connected to different gas tanks with analyzed amounts of O_2. The O_2 levels in the tanks were confirmed by use of the O_2 sensor. The relationship was used that O_2 tension in solution (C_∞) was given by:

$$C_\infty = C_0 - R/k,$$

where C_0 is the O_2 tension in the gas phase, R is the rate of O_2 consumption by the cell and k is a constant related to the efficiency of O_2 exchange in this particular geometry (*22,23*). Levels of C_∞ were changed by using tanks containing different O_2 levels (i.e., changing C_0) or varying the cell density (i.e., changing R). The effect of BMS181321 on cell respiration was assessed by measuring the rate of O_2 consumption in a closed system in the presence or absence of the ligand BMS181032 and/or ^{99m}Tc-labeled BMS181321.

Retention of BMS181321 in Cells

Cells were incubated with the tracer under aerobic or hypoxic conditions as described above for 2 hr. At this time a 10-fold excess of nonradioactive growth medium was added and cells were spun down, resuspended in 100–200 ml of nonradioactive growth medium and incubated at 37°C in suspension culture for at least 24 hr. Samples were removed from the spinner and assessed for retained activity by the spin-through-oil technique.

Imaging and Biodistribution Studies

Tumor cell lines used were KHT (fibrosarcoma), SCC-VII (squamous cell carcinoma) and RIF-1 (radiation-induced fibrosarcoma) (*24*). In vivo growth was initiated by intramuscular injection of 2–6 × 10^5 cells into the left hind leg of syngenic C3H/HeJ male mice. Over the course of 6–10 days, tumors grew to a leg diameter of 8–15 mm, corresponding to tumor weights of 500–1600 mg.

For imaging studies, unanesthetized mice were placed in a lucite jig with the leg which contained the tumor extended to the side and taped to the base plate. The jig was positioned on the face of a gamma camera equipped with a low-energy all-purpose collimator and interfaced to a computer. A magnification factor of 2.5–3 was used. During the first 5 min after injection of 2–4 MBq of the tracer via the tail vein, dynamic imaging was performed with collection of 10 images of 30 sec each. At later times, static images of 2–10 min duration were obtained. Quantification was performed by drawing a region of interest (ROI) around the tumor and comparing the counts in the ROI to those in a 20-ml standard which contained the same amount of activity as was administered to the mouse and which was imaged in the same geometry ("glass mouse"). This allowed calculation of the percent injected dose in the tumor.

At 10 min, 1, 2, 4, 6, 8 or 24 hr after injection, mice were sacrificed by cervical dislocation. A blood sample was obtained by heart puncture. The following tissues were removed, blotted dry of blood, weighed and counted: heart, lungs, liver, spleen, intestinal tract (including contents), kidneys, tail, tumor and a sample of skeletal muscle from the opposite leg. The counting tubes, including a standard equivalent to 1% of the injected dose, were assayed in a gamma well counter and the results were calculated as percent injected dose per gram tissue and percent injected dose per organ.

Tumor-to-muscle and tumor-to-blood ratios were calculated from the percent dose per gram data.

The possibility of increasing tumor hypoxia by pharmacological means was assessed by injection of hydralazine (5 mg/kg, i.p.) (*17*) or nitro-L-arginine (10 mg/kg, i.v.) (*18*) 5 or 30 min after the tracer. Groups of mice were sacrificed at 2, 4 or 6 hr after injection of the tracer.

Statistics

Data are expressed as mean ± one s.d. Comparisons between groups were performed using Student's t-test for unpaired data. Linear regression was performed by the method of least squares and the level of significance of the correlation coefficient was determined.

RESULTS

Preparation and Stability of BMS181321

The initial radiochemical purity of BMS181321 was 92.1% ± 1.4% (mean ± s.d., n = 18), but decreased with time at room temperature, particularly in preparations with higher quantities of activity. The pattern of decomposition fit a monoexponential function from which an apparent first-order decomposition rate constant, k_d, could be calculated. For preparations in which less than 750 MBq pertechnetate was added to the vial, $k_d = 0.025 \pm 0.005\ hr^{-1}$ (n = 6); when more than 1350 MBq was added, $k_d = 0.046 \pm 0.010\ hr^{-1}$ (n = 5). These rate constants correspond to half-times of 28 hr and 15 hr, respectively. The optical density of the solution (BMS181321 plus excess ligand) at 323 nm showed a decomposition half-time of 16–24 hr.

Accumulation of BMS181321 in CHO Cells

The accumulation of BMS181321 in CHO cell suspension cultures at 1×10^6 cells/ml as a function of time under aerobic or hypoxic incubation conditions at 37°C is shown in Figure 2A, expressed as the ratio of CPM in the cell pellet (C_{in}), corrected for medium carry-through, to the CPM in an equal volume of the initial external medium (C_{out}). By 5 min there was an apparent stabilization of accumulation in aerobic cells with little significant increase over the next 3–4 hr. In contrast, cells incubated in the absence of oxygen showed a continued increase in tracer accumulation with time. At this cell density the accumulation was approximately linear from 5 min to 4 hr.

The average value for C_{in}/C_{out} for aerobic cells at a 2-hr incubation time was 10.8 ± 4.2 (n = 11). This value was not statistically different when evaluated at 5-min to 4-hr incubation times. Thus the labeled 2-nitriomidazole derivative concentrated ~10-fold in aerobic cells within 5 min and did not change thereafter. The ratio of C_{in}/C_{out} for hypoxic versus aerobic cells at a 2-hr incubation time (i.e., a ratio of ratios) was 9.4 ± 3.4 in 11 separate experiments. Thus, the selective accumulation of BMS181321 in cells after 5 min incubation was hypoxia-specific.

In some experiments, especially at higher CHO cell densities ($2–4 \times 10^6$/ml), accumulation became nonlinear after 1–2 hr; a representative experiment at 3×10^6 cells/ml is shown in panel A of Figure 2. Two factors appeared to be correlated with this reduced rate of accumulation of tracer in hypoxic cells at later times. First, as seen in panel B of Figure 2, the amount of radioactivity remaining in the supernatant of hypoxic cells spun through oil diminished with time. This loss of activity could be accounted for by cellular accumulation (sequestration) of the tracer and, though only ~10% over 4 hr at 1×10^6 cells/ml, increased with cell density to ~60% at 3×10^6 cells/ml (panel B). Second, as seen in panel C, the status of radioactive material remaining in the supernatant of cellular aliquots changed with time. Initially, and in aerobic incubations as a function of time, ~90% of the radioactivity could be extracted into ethyl acetate. This was consistent with the high partition coefficient of BMS181321 (*15*). In contrast, in hypoxic cell incubations a decreasing proportion of the radioactivity present in the supernatant was extractable into ethyl acetate as a function of time. At 4 hr only ~70% of the radioactivity was extractable at 1 ×

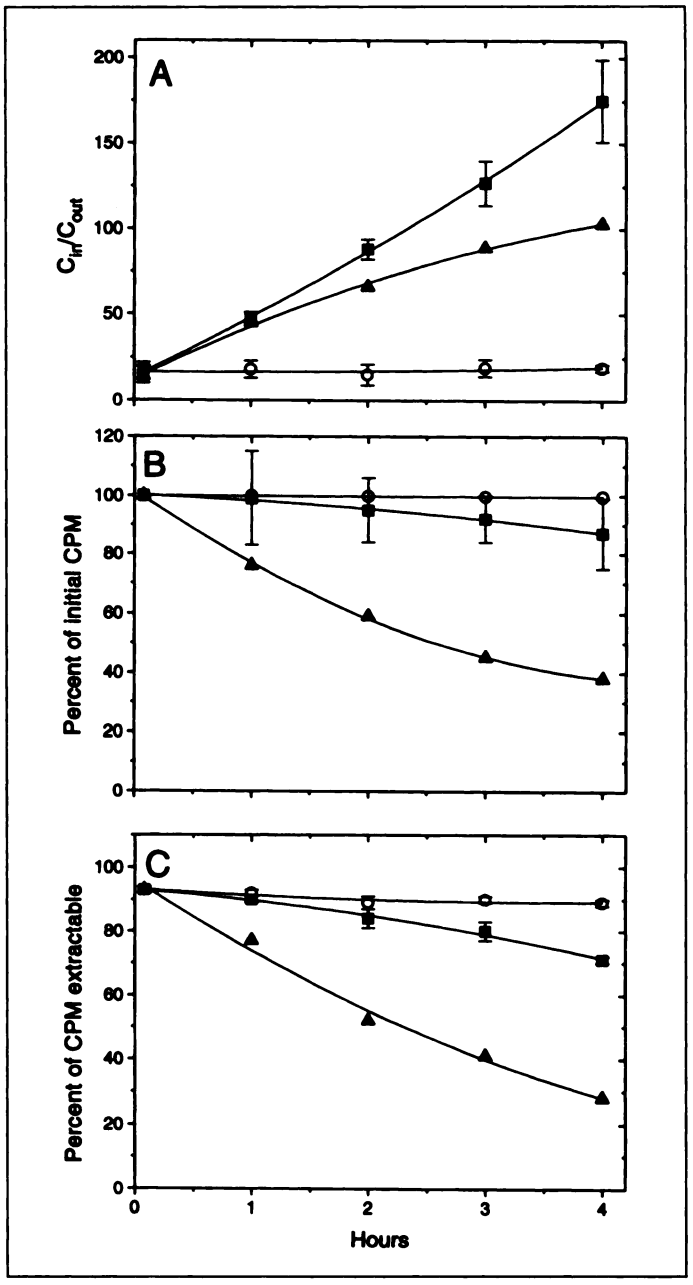

FIGURE 2. Selective accumulation of BMS181321 in extremely hypoxic versus aerobic cells. CHO cells at 1×10^6 cells/ml were incubated under aerobic (5% CO_2, 95% air; open circles) or extremely hypoxic (5% CO_2, 95% N_2, <10 ppm O_2; closed squares) gas phases in the presence of BMS181321. Data are expressed as mean of three separate experiments and error bars are standard deviations. Representative data for a single experiment using cells at 3×10^6/ml under hypoxic conditions are also shown (closed triangles). The aerobic results for this higher cell density were the same as for 1×10^6 cells/ml and are not shown. (A) Data are calculated as the ratio of CPM that are cell-associated ("inside" the cell) C_{in} to CPM in an equal volume of medium ("outside" the cell) C_{out} and plotted versus incubation time with the tracer. (B) Percent counts in cell supernatants of aerobic or hypoxic incubations relative to the aerobic 5-min point, as a function of time. (C) Percent of total counts in cell supernatants which partition into ethyl acetate phase versus PBS for aerobic or hypoxic incubations as a function of time.

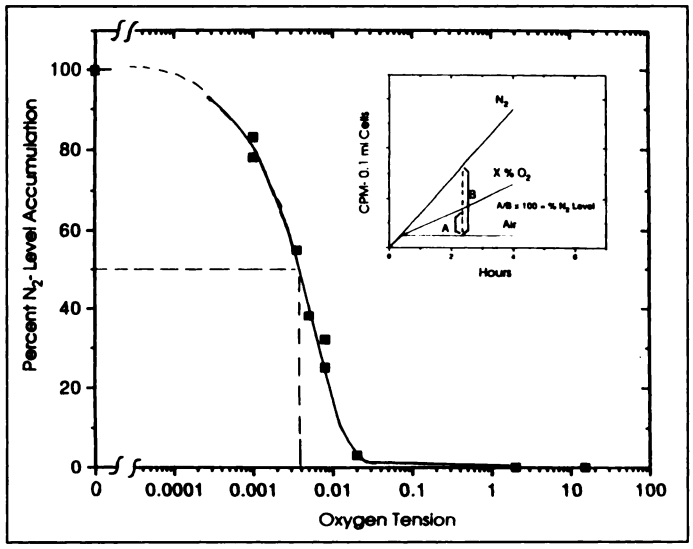

FIGURE 3. O_2 dependency of the accumulation of BMS181321 in CHO cells. The effect of different intermediate O_2 concentrations on BMS181321 accumulation was calculated relative to aerobic and extremely hypoxic (<10 ppm O_2) conditions. Each point is a single experiment with its own aerobic and extremely hypoxic accumulation curve. Percent of the extremely hypoxic accumulation was calculated as shown in the figure inset. The level of O_2 causing 50% inhibition of accumulation is shown by the dotted lines and was ~40 ppm O_2.

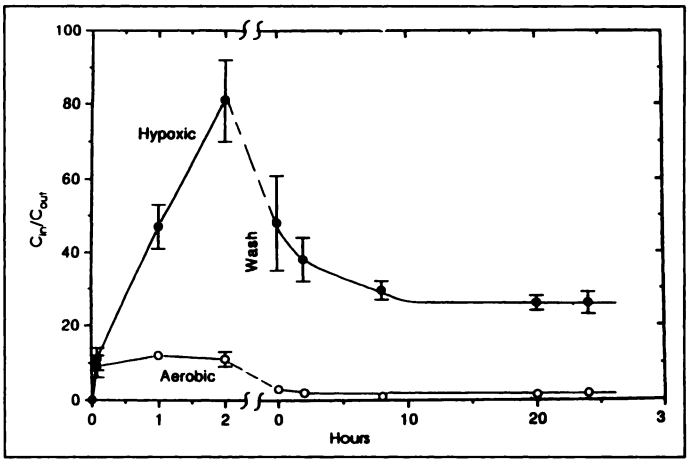

FIGURE 4. The ratio of C_{in}/C_{out} as a function of time for CHO cells incubated under aerobic or extremely hypoxic (<10 ppm O_2) conditions for 2 hr, washed, resuspended in nonradioactive medium in suspension culture and incubated for a total of 24 hr. Points are means of three experiments and error bars are standard deviations.

10^6 cells/ml. At higher cell densities the percent extractable decreased more rapidly with time under hypoxia (~30% at 3 × 10^6 cells/ml, panel C). It is possible that in hypoxic cells metabolism of the tracer occurs and altered BMS181321 and/or ^{99m}Tc is released into the medium.

Oxygen Dependency of In Vitro Accumulation

To determine the O_2 dependency of this selective uptake, a variety of analyzed gas mixtures containing known concentrations of O_2 from 5.0 to 0.35% were flowed over cell suspensions containing 1–4 × 10^6 cells/ml. The cell suspension system used has been studied previously to determine the equilibrium levels of O_2 present in solution (*22,23*). The results of these experiments are shown in Figure 3. The inset in this figure shows schematically how the effect of O_2 on tracer accumulation was determined. For each experiment, air and N_2 (<10 ppm O_2) accumulation curves were run for 0 to 4 hr and the amount of the hypoxic-specific accumulation under the intermediate O_2 gas level was expressed as a percentage of the low O_2 level accumulation, which was defined as 100%. This calculation was done at the 2-hr incubation point, since at some higher cell densities the accumulation curve for hypoxic cells became nonlinear at longer times. The level of O_2 in solution which caused a 50% inhibition of tracer accumulation was of the order of 40 ppm O_2 or 0.04 μM O_2 in solution. Thus, very low levels of O_2 were effective in inhibiting selective uptake of the tracer.

A number of control experiments were done to validate the results (data not shown). (1) Using a Yellow Springs O_2 monitor, the possible effect of the ^{99m}Tc-labeled compound on cell respiration was determined. Even at tracer plus ligand levels 100 times higher than used in these experiments there was no effect on cell respiration, either immediately or after up to 2 hr of hypoxic or aerobic incubation. This is important, since the O_2 levels in solution are dependent upon the respiration rate of the cells (*22*). (2) The rate of increase of C_{in}/C_{out} was independent of cell density, at least up to 2-hr incubation times for CHO cells, thus allowing the use of different cell densities to vary the O_2 concentration. (3) An O_2 sensor able to measure low O_2 levels was used to experimentally measure the O_2 levels predicted theoretically in selected experiments. The results of these experiments confirmed the validity of previously established techniques (*22,23*) for controlling low O_2 levels in solution. (4) Cell viability as assessed by colony-forming ability was unaffected throughout all experimental conditions (aerobic or hypoxic, plus or minus tracer) and up to 4 hr of incubation at 37°C. Thus, the observed accumulation of tracer was not altering the gross physiology or biochemistry of these cells.

Retention of Accumulated Radioactivity

To determine to what degree the tracer accumulated in aerobic or hypoxic cells was retained, cells were incubated under aerobic or hypoxic (<10 ppm O_2) conditions for 2 hr and then washed free of radioactive medium, resuspended in fresh nonradioactive medium and incubated under aerobic conditions in suspension culture under growth conditions for 0 to 24 hr. Aliquots of cells were removed throughout the experiment, spun through oil, and C_{in}/C_{out} calculated. The results are shown in Figure 4. After washing, both aerobic and hypoxic cells lost counts but the percentage loss appears larger for aerobic compared to hypoxic cells. Immediately after washing, ~60% of the counts were still cell-associated in hypoxic cells. About half of these counts were lost in the next 12 hr, but by 24 hr ~30% of the peak accumulation counts were still associated with the cells. The cell number in the spinner more than doubled over the post-wash incubation number (data not shown), again indicating that the cells, though labeled, were still viable.

Imaging and Biodistribution Studies

Dynamic gamma-camera imaging demonstrated that the tracer distributed rapidly throughout the body after intravenous injection and cleared largely through the hepatobiliary system. The liver was the organ with highest radioactivity initially and activity was quickly excreted into the intestinal tract. The absence of bladder activity suggested there was little excretion of the tracer in the urine.

These observations are reflected quantitatively in the time course of biodistribution of BMS181321 in normal tissues of tumor-bearing mice presented in Table 1. The predominance of hepatobiliary clearance is evident from the high activity in the liver and low activity in the kidneys. The liver was the organ with greatest accumulation of BMS181321 and activity remained high for at least 8 hr. In some mice the activity contained in the intestinal tract was measured; as percent of

TABLE 1
Time Course of Biodistribution of Radioactivity in Normal Tissues of Tumor-Bearing Mice after Intravenous Injection of BMS181321

Organ	%ID/g tissue						
	10 min (n = 5)	1 hr (n = 3)	2 hr (n = 11)	4 hr (n = 23)	6 hr (n = 24)	8 hr (n = 3)	24 hr (n = 4)
Blood	5.05 ± 2.94	3.34 ± 0.47	1.75 ± 0.27	2.03 ± 1.13	1.30 ± 0.29	1.48 ± 0.11	2.01 ± 0.59
Heart	2.74 ± 0.59	1.42 ± 0.36	0.61 ± 0.12	0.71 ± 0.36	0.42 ± 0.07	0.42 ± 0.02	0.59 ± 0.13
Lung	4.28 ± 1.97	2.51 ± 0.60	1.40 ± 0.21	1.50 ± 0.56	0.97 ± 0.13	1.05 ± 0.06	1.11 ± 0.13
Liver	14.01 ± 3.12	14.10 ± 2.28	8.79 ± 3.05	8.79 ± 2.55	7.10 ± 1.23	7.94 ± 0.55	3.24 ± 0.47
Spleen	2.72 ± 0.92	1.34 ± 0.20	0.82 ± 0.21	0.82 ± 0.32	0.60 ± 0.07	0.63 ± 0.05	0.74 ± 0.19
Kidney	6.44 ± 0.81	3.26 ± 0.51	2.26 ± 0.68	2.23 ± 0.50	1.60 ± 0.33	1.42 ± 0.02	0.93 ± 0.14
Skeletal muscle	1.43 ± 0.39	0.27 ± 0.07	0.19 ± 0.05	0.16 ± 0.07	0.12 ± 0.04	0.14 ± 0.02	0.13 ± 0.03

Each value is mean ± s.d. for number of mice.

injected dose, these values were 60% at 2 hr (n = 2), 58% ± 2% at 4 hr (n = 3) and 37% ± 18% at 6 hr (n = 18). The lower value at 6 hr was due to elimination of feces from the body and the larger s.d. at that time point was due to variability in amount eliminated. Radioactivity cleared from the blood relatively quickly to a plateau of ~4% of the injected dose recovered in the blood pool (~2% ID/g, ~2 ml blood volume) from 2 hr onward.

The time course of tumor localization of BMS181321 is shown in Table 2 and tumor-to-muscle ratios are plotted in Figure 5. Absolute uptake in KHT tumors was highest at 10 min after injection, then dropped somewhat and remained relatively constant from 2 to at least 8 hr postinjection, after which it decreased by 24 hr. Tumor-to-muscle ratios increased until 4 hr, followed by a plateau to at least 8 hr. Based on these results with KHT tumors, a more limited time course was studied in two other types of tumor. SCC-VII and RIF-1 tumors showed absolute uptakes and tumor-to-muscle ratios not significantly different from those obtained with KHT tumors.

The image presented in Figure 6 is an anterior view obtained 2 hr after intravenous administration of 3.49 MBq BMS181321 to a mouse bearing a 1.1-g SCC-VII tumor in its left hind leg. The intense localization of radioactivity in the abdomen makes it necessary to adjust the upper threshold in order to be able to visualize the tumor in the leg, which is extended to the right side of the image. When this animal was sacrificed, the tumor was found to contain 0.51% of the injected dose per gram and the tumor-to-muscle ratio was 2.88.

It has previously been reported that the hypoxic cell fraction in experimental solid tumors increases with tumor size (*2*). The effect of tumor weight on localization of BMS181321 (tumor-to-muscle ratio at 4–6 hr after injection) is shown in Figure 7. For KHT tumors (n = 30), linear regression analysis produced a highly significant correlation between tumor weight and tumor/muscle ratio (slope = 2.5, r = 0.68, $p < 0.001$). For SCC-VII and RIF-1 tumors the slopes were also positive but the correlation coefficients did not reach significance, possibly due to the narrower range of tumor sizes and smaller number of data points. It should be noted that these positive slopes are not simply due to greater absolute uptake in larger tumors, because tumor-to-muscle ratios are calculated from the percent dose per gram in tumor and muscle.

Pharmacological Modulation of Tumor Hypoxia

It has previously been demonstrated that injection of hydralazine or nitro-L-arginine produces metabolic changes in tumors consistent with increased hypoxia (*17,18*). As shown in Table 3, injection of hydralazine or nitro-L-arginine produced a significant increase in tumor levels of BMS181321. Increases produced by hydralazine were greater than those produced by nitro-L-arginine in all three tumor types at the single dose levels studied. These data were obtained at 6 hr after injection; statistically significant differences were also observed at 2 and 4 hr after injection (data not shown).

DISCUSSION

When BMS181321 is prepared by adding pertechnetate to the kit, the labeling efficiency of BMS181321 reaches a maximum

TABLE 2
Time Course of Tumor Localization of Radioactivity in Mice Bearing KHT, SCC-VII or RIF-1 Tumors after Intravenous Injection of BMS181321

	10 min	1 hr	2 hr	4 hr	6 hr	8 hr	24 hr
KHT tumor	n = 3	n = 3	n = 9	n = 12	n = 13	n = 3	n = 3
% dose/g	1.91 ± 0.29	0.73 ± 0.22	0.55 ± 0.08	0.53 ± 0.26	0.42 ± 0.11	0.52 ± 0.05	0.31 ± 0.10
% dose/tumor	1.73 ± 0.35	0.63 ± 0.28	0.63 ± 0.22	0.52 ± 0.42	0.45 ± 0.20	0.50 ± 0.04	0.34 ± 0.28
Tumor-to-muscle	1.44 ± 0.34	2.72 ± 0.15	2.63 ± 0.57	3.53 ± 1.80	3.94 ± 1.08	3.92 ± 0.87	2.47 ± 0.61
SCC tumor	n = 2		n = 2	n = 7	n = 7		
% dose/g	1.65		0.47	0.62 ± 0.15	0.47 ± 0.13		
% dose/tumor	1.50		0.53	0.54 ± 0.17	0.35 ± 0.15		
Tumor-to-Muscle	1.12		3.00	4.21 ± 0.63	3.34 ± 0.95		
RIF-1 tumor			n = 6	n = 3	n = 6		
% dose/g			0.47 ± 0.06	0.50 ± 0.16	0.45 ± 0.11		
% dose/tumor			0.49 ± 0.11	0.32 ± 0.11	0.39 ± 0.15		
Tumor-to-Muscle			2.88 ± 0.27	3.54 ± 1.18	3.49 ± 0.89		

Each value is mean ± s.d. for number of mice or mean for two mice.

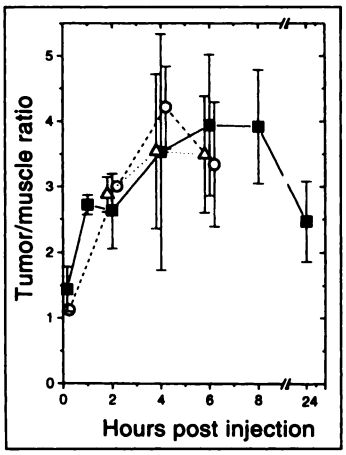

FIGURE 5. Effect of time after injection of ^{99m}Tc-BMS181321 on tumor-to-muscle ratio. Tumor type: KHT = solid squares; SCC-VII = open circles; RIF-1 = open triangles.

within 10 min, then slowly declines at a rate dependent upon the amount of activity added, resulting in half-times of 15–28 hr. The optical density of the absorption peak of the 2-nitroimidazole in the BMS181321 preparation or BMS181032 solution monitored at 323 nm decays exponentially with a half-time in a similar range. Neither the radiochemical nor the chemical instability is a significant problem for the interpretation of the present results.

In Vitro Accumulation Studies

BMS181321 is selectively accumulated in CHO cells under extremely hypoxic incubation conditions. As seen in Figure 2, this accumulation appears to start within 5 min of addition of tracer, and increases linearly up to at least 4 hr. When the same experiment was done at 4°C, there was no accumulation of counts with time and hypoxic cell accumulation was similar to that for aerobic cells in Figure 2, suggesting that an enzymatic process is involved in tracer accumulation (data not shown).

After 2 hr, the average C_{in}/C_{out} value for aerobic cells was ~11. This was consistent with the measured octanol-to-water partition coefficient for BMS181321 of ~40 (data not shown) and indicated a concentrating of the tracer in the cell in the initial uptake phase. After 2 hr, the accumulation was 9-fold higher in hypoxic versus aerobic cells. In previous studies with CHO cells and the ^{14}C-labeled 2-nitroimidazole misonidazole, the C_{in}/C_{out} value for aerobic cells was reported to be ~0.9 (*25*). The partition coefficient for this 2-nitroimidazole is 0.4, which is much less lipophilic than BMS181321. Additionally, the selective accumulation of misonidazole in hypoxic versus aerobic cells, though approximately linear up to 7 hr, was only 2-fold at 2 hr (*25*).

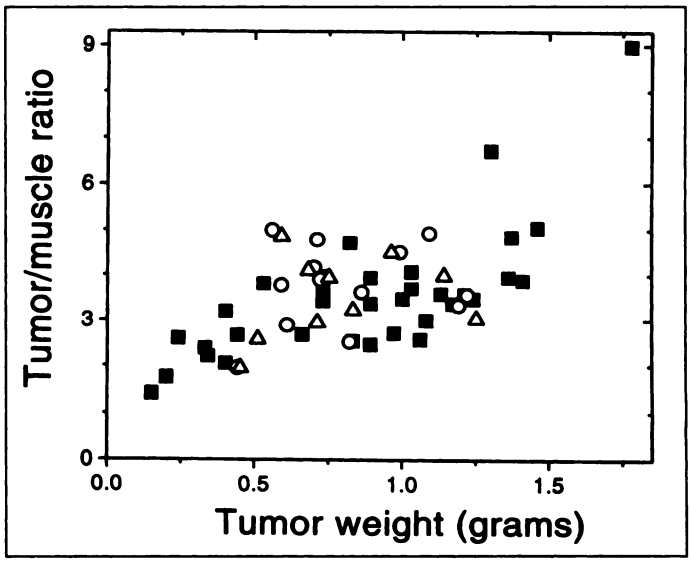

FIGURE 7. Effect of tumor weight on tumor-to-muscle ratio in mice killed 4–6 hr after injection of ^{99m}Tc-BMS181321. Tumor type: KHT, solid squares; SCC-VII, open circles; RIF-1, open triangles.

Cell Line and Cell Density Effects

In a limited number of studies with a human cell line (HeLa), the behavior of BMS181321 was similar to that observed in CHO cells, but HeLa cells appeared to accumulate radioactivity at a rate ~2 times faster than CHO cells (data not shown). Again, there was depletion of radioactivity from the supernatant in hypoxic cell cultures with little depletion in aerobic cultures and a very striking decrease in the ability of the radioactivity in the supernatant of hypoxic cells to be extracted into ethyl acetate. These results suggest quantitative differences in the rate of BMS181321 accumulation and metabolism in CHO and HeLa cell lines.

Interestingly, the apparent 2-to-4-fold enhanced metabolism of BMS181321 in hypoxic HeLa versus CHO cells was also seen previously for ^{14}C-misonidazole (*25*). Since ^{14}C-misonidazole has a low specific activity, studies were done at high drug concentration (0.5–20 m*M*) compared to the present studies and at these higher drug concentrations selective toxicity to hypoxic cells was observed (*20*). No toxicity was observed to aerobic or hypoxic cells with BMS181321, consistent with the low concentration, ~2 μM, of the tracer plus ligand in the present experiments.

Nonlinear accumulation of radioactivity observed at cell densities $>1 \times 10^6$/ml for both CHO and HeLa cells (data not shown) appeared to be due to both depletion of radioactivity from the external medium (Fig. 2, panel B) and alteration of the state of the tracer that remains (panel C). Koch et al. have measured the rate of consumption of μM levels of misonidazole in rat 9L cells under incubation conditions of extreme hypoxia and arrived at a rate of consumption of 7.4×10^{-19} moles/cell/sec (*26*). If CHO cells metabolized BMS181321 at this rate, one can calculate that 1×10^6 cells/ml would consume all the tracer in 40 min, which is clearly not the case. From Figure 2 an estimate can be made of the rate of consumption of BMS181321 over the first hour of 6.8×10^{-20} moles/cell/sec, about one-tenth the rate of misonidazole consumption in 9L cells. Clearly, it will be of interest to determine to what degree

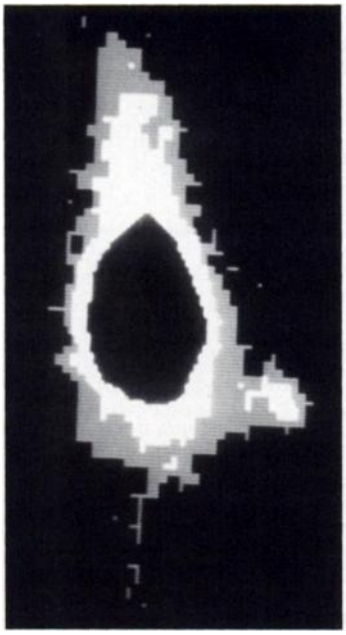

FIGURE 6. Gamma-camera image of a mouse bearing a transplanted SCC-VII tumor in the left hind leg obtained at 2 hr after injection of 3.49 MBq ^{99m}Tc-BMS181321. The image is an anterior view; the tumor is in the lower right portion of the image. The upper threshold has been reduced to mask activity in the abdomen to allow visualization of the tumor.

TABLE 3
Effect of Modulation of Tumor Hypoxia by Injection of Hydralazine or Nitro-L-arginine 30 Minutes after BMS181321

Tumor type	Modulator	Modulator n	Modulator %ID/g	Control n	Control %ID/g	Student's t-test
KHT	Hydralazine	5	1.00 ± 0.15	4	0.44 ± 0.04	$p < 0.001$
KHT	Nitro-L-arginine	4	0.86 ± 0.03	4	0.50 ± 0.06	$p < 0.001$
SCC-VII	Hydralazine	8	0.91 ± 0.31	6	0.40 ± 0.09	$p < 0.005$
SCC-VII	Nitro-L-arginine	7	0.63 ± 0.20	6	0.40 ± 0.09	$p < 0.025$
RIF-1	Hydralazine	3	0.70 ± 0.10	4	0.46 ± 0.07	$p < 0.025$
RIF-1	Nitro-L-arginine	5	0.63 ± 0.10	7	0.45 ± 0.11	$p < 0.025$

Each value is mean ± s.d. for number of mice killed at 6 hr postinjection.

these metabolic rates are dependent on cell type, drug structure and partition coefficient. As has been pointed out by Koch et al., the metabolism of nitroheterocycles at levels used for measuring tissue hypoxia may have to be considered in assessing the degree they can quantitatively predict the extent of tumor hypoxia (*26*).

Oxygen Dependency and Stability

The selective accumulation of BMS181321 in extremely hypoxic cells (<10 ppm O_2) was sensitive to low levels of O_2 with a K_m of 40 ppm of O_2 and an estimated dissolved O_2 level of 0.04 μM in the growth medium (Fig. 3). This exquisite sensitivity to O_2 has been previously observed for misonidazole with similar low levels of O_2 inhibiting drug toxicity and altering the rates of misonidazole metabolism (*20*). It must be stressed that large corrections were necessary for the fact that the cells were consuming O_2 and at low gas-phase O_2 levels there was a much lower O_2 tension in solution than would be predicted from simple equilibration of the gas phase with a cell-free aqueous solution (*23*). As has been discussed previously, this suggests that 2-nitroimidazole accumulation in cells occurs at O_2 levels at which cells are fully radiobiologically hypoxic (i.e., <1 μM O_2 in solution) (*27*). In many ways it would be useful to be able to design hypoxic cell markers which would be accumulated at different O_2 tensions so that the degree or level of hypoxia could be mapped, but at present it is not obvious how this can be done rationally (*28*).

In analogy with other 2-nitroimidazoles, and supported by preliminary reports (*13,29*), it is assumed that the accumulation of BMS181321 in hypoxic cells is due to selective reduction of the nitro group to the radical anion, the O_2-inhibitable stage, and further reduction to the nitroso or perhaps hydroxylamine stage at which rearrangement occurs to a reactive intermediate which can rapidly bind to nucleophilic sites on proteins, nucleic acids and other cellular macromolecules (*30*). To date, however, the nature of the accumulated radioactivity in cells has not been determined. Trapping of the tracer has been suggested by recent work of others (*15*). Certainly some fraction of the radioactivity is selectively retained in hypoxic cells and a lower level in aerobic cells after incubation with BMS181321, washing and culturing of cells in the absence of additional tracer (Fig. 4). The nature of this material is not known at the present time. Nevertheless, at incubation times up to 24 hr, and limited data up to 40 hr (not shown), 30% or more of the counts taken up 24 hr earlier remain associated with the cell. This can be compared to washout studies with misonidazole in which a half-life for cell-associated material after a wash was 50–55 hr (*31*).

Biodistribution and Imaging Studies

Following intravenous administration to mice, the high partition coefficient of BMS181321 plays an important role in the biodistribution of the tracer (*15*). Delivery to all tissues is rapid, followed by washout and extensive hepatobiliary clearance. Initially, the tracer clears from the blood relatively quickly, with only ~10% of the dose remaining in the blood pool 10 min after injection and ~4% at 2 hr. This blood level, however, is not negligible and may contribute to the relatively modest tumor/muscle ratios obtained. Moreover, as can be seen from the data in Tables 1 and 2, tumor-to-blood ratios were <1 at all time points. The liver is the organ containing the highest amount of radioactivity, ~14% of the dose after 10 min and ~8% after 8 hr. The other organs clear more quickly. The extensive hepatobiliary clearance means there are high levels of background activity in the abdomen, making detection of adjacent tumors difficult.

Tumor levels of radioactivity following administration of BMS181321 varied as a function of time after injection (Fig. 5) and tumor weight (Fig. 7), but showed no significant differences among the three types of tumors studied. Although the RIF-1 tumor line is reported to have a lower hypoxic fraction than KHT and SCC-VII tumors (*2,24*), recent measurements at our institution of hypoxic fraction by paired survival curve techniques in the tumor types used in these experiments suggest that the current strain of RIF-1 does not have a significantly lower hypoxic fraction than KHT and SCC-VII (*32*).

The tracer is not trapped irreversibly; activity in the tumor slowly declines with time and tumor-to-muscle ratios reach a plateau followed by a decline (Fig. 5). This suggests there will be an optimal time window for imaging and that window will occur relatively early, which is advantageous given the 6-hr half-life of ^{99m}Tc. The observation of limited washout of activity from tumors in vivo parallels the results reported above in tumor cell suspensions in vitro (Fig. 4). Washout of IAZA from tumors in vivo has also been reported (*6*).

Further evidence for the role of hypoxia in localization of BMS181321 was obtained in the modulator studies in which a pharmacologically induced increase in the degree of hypoxia resulted in significantly more of the tracer localizing in the tumor (Table 3). Results were obtained at a single dose level of hydralazine and nitro-L-arginine, and further investigation is required to determine the relative potency of these two agents. These doses of modulator produced no obvious change in behavior of the animals and had little effect on the distribution of radioactivity in normal tissues. The kidney was the only tissue to contain significantly higher radioactivity after administration of hydralazine. With nitro-L-arginine, activity tended

TABLE 4
Octanol/Water Partition Coefficient (p), Tissue Uptake and Tumor-to-Tissue Ratio at 2 Hours for Some Labeled 2-Nitroimidazoles

Compound	p	%ID/g			Tumor/ Blood ratio	Tumor/ Muscle ratio	Tumor model	Reference
		Tumor	Blood	Muscle				
^{3}H-misonidazole	0.43	1.37 ± 0.45	0.73 ± 0.23	0.89 ± 0.33	1.88	1.54	C3H mice, KHT tumor	33
^{3}H-FMISO	0.40	1.29 ± 0.07	0.98 ± 0.07	0.91 ± 0.10	1.32	1.42	BALB/c mice, EMT-6 tumor	33
^{125}I-IAZA	4.98	2.55 ± 1.56	0.91 ± 0.20	0.69 ± 0.29	2.80	3.70	BALB/c mice, EMT-6 tumor	6
^{99m}Tc-BMS181321	~40	0.55 ± 0.08	1.75 ± 0.27	0.19 ± 0.05	0.31	2.63	C3H mice, KHT tumor	This work

to be higher in the liver and was significantly higher in the intestinal tract at 6 hr after injection, presumably due to decreased intestinal motility (data not shown).

Comparison With Previous Results

It is useful to compare the present results to previous results obtained with FMISO (*33*) and IAZA (*6*). In mouse-tumor systems both these compounds show superior pharmacokinetic behavior to BMS181321 in terms of an increased tumor/blood ratio at 2–24 hr postinjection. As seen in Table 4, which presents a comparison of data obtained at 2 hr postinjection, both of these compounds show higher tumor localization and lower blood levels than the present compound. This may be due in part to the lower octanol/water partition coefficients of FMISO and IAZA compared to BMS181321. The tumor-to-muscle ratios do not differ substantially among the tracers and this ratio for BMS181321 is actually higher than for FMISO, with which clinical imaging is performed within 2 hr after injection due to the short half-life of ^{18}F. The extent to which the low tumor-to-blood ratios obtained with BMS181321 are a limitation for clinical imaging will likely depend on the location of the tumor to be imaged. The detectability of tumors depends on both the absolute amount of radioactivity in the tumor and the tumor-to-background ratio; whether these parameters are adequate for clinical imaging with BMS181321 is not yet clear. In addition, the degree of retention of the ^{99m}Tc label in BMS181321 in vivo in various body tissues has yet to be determined. In particular, it will be important to evaluate ^{99m}Tc-labeled 2-nitroimidazole analogs with lower partition coefficients to see if they show superior tumor-to-background ratios, as well as to investigate a variety of human tumor types to assess the generality of the present work.

These apparent advantages of FMISO and IAZA must be weighed against some of their limitations. Use of FMISO is restricted to centers with a PET camera, access to cyclotron-produced ^{18}F and radiochemistry facilities. IAZA is labeled with ^{123}I, which is expensive and inconvenient to obtain, the labeling yield is only ~50%, purification by HPLC is required, and the injected dose is limited to 370 MBq (10 mCi).

In contrast, BMS181321 is labeled with ^{99m}Tc, which is routinely available and relatively inexpensive. It is prepared from a kit without the need for purification, the complex has a high partition coefficient allowing it to readily cross membranes, and doses of 740–1110 MBq (20–30 mCi) could potentially be injected, limited by dosimetry rather than practicalities and expense. Finally, it can be imaged with routinely available planar and SPECT gamma cameras whose resolution approaches that of PET systems, although tumors smaller than this resolution limitation may contain hypoxic cells. Thus, the development of BMS181321 and analogs of it could represent an important advance in nuclear medicine, allowing routine imaging of hypoxia in tumors and areas at risk of infarction in the brain and heart (*14–16,34*).

ACKNOWLEDGMENTS

We thank Bob Kuba for technical assistance with the in vivo studies. This work was supported by a grant from the Bristol-Myers Squibb Pharmaceutical Research Institute and operating grants from the Medical Research Council and National Cancer Institute of Canada. This work was presented in part at the 42nd Annual Meeting of the Society of Nuclear Medicine, Minneapolis, MN, June 14, 1995.

REFERENCES

1. Gray LH, Conger AD, Ebert M, Hornsey S, Scott OCA. Concentration of oxygen dissolved in tissues at time of irradiation as a factor in radiotherapy. *Br J Radiol* 1953;26:638–648.
2. Moulder JE, Rockwell S. Tumor hypoxia: its impact on cancer therapy. *Cancer Metastasis Rev* 1987;5:313–341.
3. Chapman JD. Hypoxic sensitizers: implications for radiation therapy. *N Engl J Med* 1979;301:1429–1432.
4. Koh W-J, Rasey JS, Evans ML, et al. Imaging of hypoxia in human tumors with [^{18}F]-fluoromisonidazole. *Int J Radiat Oncol Biol Phys* 1991;22:199–212.
5. Martin GV, Caldwell JH, Graham MM, et al. Noninvasive detection of hypoxic myocardium using fluorine-18-fluoromisonidazole and positron emission tomography. *J Nucl Med* 1992;33:2202–2208.
6. Mannan RH, Somayaji VV, Lee J, Mercer JR, Chapman JD, Wiebe LI. Radioiodinated 1-(5-iodo-5-deoxy-beta-D-arabinofuranosyl)-2-nitro-imidazole (Iodoazomycin arabinoside: IAZA): a novel marker of tissue hypoxia. *J Nucl Med* 1991;32:1764–1770.
7. Parliament MB, Chapman JD, Urtasun RC, et al. Noninvasive assessment of human tumor hypoxia with ^{123}I-iodoazomycin arabinoside: preliminary report of a clinical study. *Br J Cancer* 1992;65:90–95.
8. Groshar D, McEwan AJB, Parliament MB, et al. Imaging tumor hypoxia and tumor perfusion. *J Nucl Med* 1993;34:885–888.
9. Biskupiak JE, Grierson JR, Rasey JS, Martin GV, Krohn KA. Synthesis of an (iodovinyl)misonidazole derivative for hypoxia imaging. *J Med Chem* 1991;34:2165–2168.
10. Martin GV, Biskupiak JE, Caldwell JH, Rasey JS, Krohn KA. Characterization of iodovinylmisonidazole as a marker for myocardial hypoxia. *J Nucl Med* 1993;34:918–924.
11. Linder KE, Cyr J, Chan YW, et al. Chemistry of a Tc-PnAO-nitroimidazole complex that localizes in hypoxic tissue [Abstract]. *J Nucl Med* 1992;33:919.
12. DiRocco RJ, Bauer A, Kuczynski BL, et al. Imaging regional hypoxia with a new technetium-labeled imaging agent in rabbit myocardium after occlusion of the left anterior descending coronary artery [Abstract]. *J Nucl Med* 1992;33:865.
13. Linder KE, Chan YW, Cyr JE, Malley MF, Nowotnik DP, Nunn AD. TcO(PnAO-1-(2-nitroimidazole)) [BMS181321], a new technetium-containing nitroimidazole complex for imaging hypoxia: synthesis, characterization and xanthine oxidase-catalyzed reduction. *J Med Chem* 1994;37:9–17.
14. DiRocco RJ, Kuczynski BL, Pirro JP, et al. Imaging ischemic tissue at risk of infarction during stroke. *J Cereb Blood Flow Metab* 1993;13:755–762.
15. Rumsey WL, Cyr JE, Raju N, Narra RK. A novel [^{99m}]Tc-labeled nitroheterocycle capable of identification of hypoxia in heart. *Biochem Biophys Res Commun* 1993; 193:1239–1246.
16. Kusuoka H, Hashimoto K, Fukuchi K, Nishimura T. Kinetics of a putative hypoxic tissue marker, technetium-99m-nitroimidazole (BMS181321), in normoxic, hypoxic, ischemic and stunned myocardium. *J Nucl Med* 1994;35:1371–1376.
17. Wood PJ, Stratford IJ, Sansom JM, Cattanach BM, Quinney RM, Adams GE. The response of spontaneous and transplantable murine tumors to vasoactive agents measured by ^{31}P magnetic resonance spectroscopy. *Int J Radiat Oncol Biol Phys* 1992;22:473–476.
18. Wood PJ, Stratford IJ, Adams GE, Szabo C, Thiemermann C, Vane JR. Modification of energy metabolism and radiation response of a murine tumor by changes in nitric oxide availability. *Biochem Biophys Res Commun* 1993;192:505–510.
19. Cyr JE, Linder KE, Nowotnik DP. Quality control of TcOPnAO-1-2nitro (BMS181321): paper chromatography and Sep Pak™ methods for determination of radiochemical purity, ^{99m}Tc-microcolloid and ^{99m}Tc-DTPA in radiopharmaceutical kits [Abstract]. *J Nucl Med* 1994;35:138P.
20. Taylor YC, Rauth AM. Oxygen tension, cellular respiration and redox state as variables influencing the cytotoxicity of the radiosensitizer misonidazole. *Radiat Res* 1982;91:104–123.
21. Ballinger JR, Cowan DSM, Boxen I, Zhang ZM, Rauth AM. Effect of hypoxia on the

accumulation of technetium-99m-glucarate and technetium-99m-gluconate by Chinese hamster ovary cells in vitro. *J Nucl Med* 1993;34:242–245.
22. Marshall RS, Koch CJ, Rauth AM. Measurement of low levels of oxygen and their effect on respiration in cell suspensions maintained in an open system. *Radiat Res* 1986;108:91–101.
23. Whillans DW, Rauth AM. An experimental and analytical study of oxygen depletion in stirred cell suspensions. *Radiat Res* 1980;84:97–114.
24. Bristow RG, Hardy PA, Hill RP. Comparison between in vitro radiosensitivity and in vivo response of murine tumor cell lines. I. Parameters of in vitro radiosensitivity and endogenous cellular glutathione levels. *Int J Radiat Oncol Biol Phys* 1990;18:133–145.
25. Taylor YC, Rauth AM. Differences in the toxicity and metabolism of the 2-nitroimidazole misonidazole (Ro07-0582) in HeLa and Chinese hamster ovary cells. *Cancer Res* 1978;38:2745–2752.
26. Koch CJ, Giandomenico AR, Iyengar CW. Bioreductive metabolism of AF-2[2-(2-furyl)-3-(5-nitro-2-furyl)acrylamide] combined with 2-nitroimidazoles. Implications for use as hypoxic cell markers. *Biochem Pharmacol* 1993;46:1029–1036.
27. Marshall RS, Rauth AM. Oxygen and exposure kinetics as factors influencing the cytotoxicity of porfiromycin, a mitomycin C analog, in Chinese hamster ovary cells. *Cancer Res* 1988;48:5655–5659.
28. Rauth AM, Marshall RS, Kuehl BL. Cellular approaches to bioreductive drug mechanisms. *Cancer Metastasis Rev* 1993;12:153–164.
29. Chan YW, Linder KE, Jayatilak PG, et al. In-vitro studies of the hypoxic retention of a novel technetium-99m labeled nitroimidazole in rat heart [Abstract]. *J Nucl Med* 1994;35:18P–19P.
30. McClelland RA, Panicucci R, Rauth AM. Products of the reduction of 2-nitroimidazoles. *J Am Chem Soc* 1987;109:4308.
31. Chapman JD, Ball K, Lee J. Characteristics of the metabolism-induced binding of misonidazole to hypoxic mammalian cells. *Cancer Res* 1993;43:1523–1528.
32. Kavanaugh M-C, Sun A, Hu Q, Hill RP. Comparing techniques of measuring tumor hypoxia in different murine tumors: Eppendorf pO_2 histograph, [^{3}H]misonidazole binding and paired survival assay. *Radiat Res* 1996;145:491–500.
33. Grunbaum Z, Freauff SJ, Krohn KA, Wilbur DS, Magee S, Rasey JS. Synthesis and characterization of congeners of misonidazole for imaging hypoxia. *J Nucl Med* 1987;28:68–75.
34. Rumsey WL, Patel B, Linder KE. Effect of graded hypoxia on retention of technetium-99m-nitroheterocycle in perfused rat heart. *J Nucl Med* 1995;36:632–636.

Targeting of Glucose Transport Proteins for Tumor Imaging: Is It Feasible?

Carol Anne Nelson, Qian Jennifer Wang, Jeffrey Paul Bourque and Paul David Crane
DuPont Merck Pharmaceutical Company, North Billerica, Massachusetts

If glucose transport proteins (Glut) are elevated in tumors they may be good targets for tumor imaging. For targeting, the overexpression of Glut should be a general characteristic of tumors. Moreover agents which bind to Glut should accumulate selectively in tumors. **Methods:** To test this, we quantitated Glut in isolated membranes from three human tumor xenografts, two murine tumor models and normal murine tissues using direct binding studies. Additionally, the biodistribution of two compounds which bind to Glut, 7-[[(2-(3-((^{125}I-p-hydroxyphenyl)propionyl)aminoethyl)amino]carbonyl]-7-desacetyl-forskolin ([^{125}I]HPP forskolin) and [^{3}H]cytochalasin B, were studied in a tumor model which overexpressed Glut. **Results:** There were multiple classes of binding sites for [^{3}H]cytochalasin B and a percentage of these sites were competitive with D-glucose but not L-glucose. The rank potency and IC_{50} values for [^{3}H]cytochalasin B binding were: 2-deoxy-D-glucose (4.5 m*M*) ≥ D-glucose (7 m*M*) > mannose (25 m*M*) > galactose (35 m*M*) > rhamnose (1–3 m*M*) > sorbitol (1–3 m*M*) and were similar to reported values for transport. The average density of Glut in four tumor models and normal tissues was between 0.7 and 4 pmole/mg protein, but K_d values were not significantly different (69 n*M*). In LX-1 human lung tumor xenograft (LX-1) Glut were 10-to-20-fold higher than other tissues (21.6 ± 0.6 pmole/mg protein, $p < 0.01$). Immunostaining of Glut-1 was more prominent in LX-1 than other xenograft tumors, consistent with the binding data. Glut density was highest in poorly vascularized regions suggesting that Glut upregulation was related to a biofeedback mediated event. Iodine-125 HPP-forskolin and [^{3}H]cytochalasin B did not localize in LX-1 tumors. **Conclusion:** Glut overexpression was not a common characteristic of the five tumors tested. Iodine-125 HPP-forskolin and [^{3}H]cytochalasin B did not localize in LX-1 tumors, indicating that these agents did not target tumors with upregulated Glut. Results suggest that Glut are not a promising target for tumor imaging.

Key Words: glucose transport proteins; tumor imaging; PET
J Nucl Med 1996; 37:1031–1037

Received Apr. 20, 1995; accepted Sep. 13, 1995.
For correspondence or reprints contact: Carol Anne Nelson, PhD, Diatide, 9 Delta Dr., Londonderry, NH 03053.

High glucose metabolism has long been recognized as a distinguishing characteristic of tumors. Historically, tumors placed in solution were found to take up large concentrations of glucose relative to normal tissues (*1*). The accumulation of 2-DG analogs such as [^{18}F]FDG has been used to image tumors with PET (*2–4*). The phosphorylated form of [^{18}F]FDG is trapped intracellularly because it is not a good substrate for cellular export or further metabolism (*5*). The high concentration of [^{18}F]FDG in tumors has been attributed to increased hexokinase activity (*6*), decreased phosphatase activity (*5*) or high concentrations of Glut (*7–10*). In situ hybridization studies from several groups have shown overexpression of Glut mRNA and transcript in a variety of human primary tumors (*7,9–11*). In addition, several studies have linked the transformation of cells to a direct upregulation of Glut (*12–15*). From these studies, it is generally accepted that the upregulation of Glut is a common characteristic of tumor biology. It has been suggested that agents which bind to Glut, such as labeled 3-radioiodo-phloretin, may serve as alternative tumor imaging agents to ^{18}F-FDG (*16*). Dissociation constants for the binding of [^{125}I]HPP forskolin and [^{3}H]cytochalasin B to Glut (100 n*M*) are higher than dissociation constants for phloretin (1 u*M*) (*16–18*), and thus chosen for this study. Two approaches were taken to determine whether Glut could be targeted for tumor imaging: (1) the concentrations of Glut were estimated in five tumors, and six normal tissues; and (2) the biodistribution of [^{125}I]HPP forskolin and [^{3}H]cytochalasin B was measured in tumor xenografts that overexpressed Glut.

MATERIALS AND METHODS

Tumor Xenografts

Female Crl:CD-1®-nuBr outbred isolator maintained nude mice (10–12 wk old) were used for all human tumor xenografts. The MX-1 human breast carcinoma xenograft and the LX-1 human lung carcinoma xenograft were both established by B. Giovanella of the Stehlin Foundation of Houston, Texas. Xenografts were